Seventh International Conference on Computational Fluid Dynamics (ICCFD7), Big Island, Hawaii, July 9-13, 2012

ICCFD7-1404

Deterministic Solver for Rarefied Flow Problems of Gases of Arbitrary Statistics Based on the Semiclassical Boltzmann - BGK Equation

B. P. Muljadi*, J. Y. Yang*
Corresponding author: muljadi.bp@gmail.com

* Institute of Applied Mechanics, National Taiwan University, TAIWAN

July 7, 2012

Abstract: A direct method for solving rarefied flow of gases of arbitrary particle statistics is presented. The method is based on semiclassical Boltzmann equation with BGK relaxation time approximation. The discrete ordinate method is first applied to render the Boltzmann equation into hyperbolic conservation laws with source terms, then classes of explicit and implicit time integration schemes are applied to evolute the discretized distribution function. The method is tested on both transient and steady flow problems of gases of arbitrary statistics at varying relaxation times.

Keywords: Semiclassical Boltzmann-BGK Equation, Gases of Arbitrary Particle Statistics, WENO, TVD

1 Introduction

In kinetic theory of gases, the Boltzmann equation has been widely used to describe various transport phenomena in classical rarefied gas covering wide range of flow parameters such as Reynolds number, Mach number and Knudsen number. The Chapman-Enskog expansion method is usually applied to the Boltzmann equation to derive closed set hydrodynamic transport equations that apply to a broad range of flow regimes, see [1]. In analogy to the classical Boltzmann equation, a semiclassical Boltzmann equation, which generalizes the collision term in order to treat the collision of particles of quantum statistics, has been developed; For detail, readers may refer to [2, 3]. Hydrodynamic behaviour of quantum gases has been the subject of some prominent researches, see [4, 5, 6], and the application of quantum Boltzmann hydrodynamic equations have been implemented in the analysis of electron flows in quantum semiconductor devices, such as in the works of [7, 8, 9]. In recent years, due to the rapid advancements of microtechnology and nanotechnology, the device or structure characteristic length scales become comparable to the mean free path and the wavelength of energy and information carriers (mainly electrons, photons, phonons, and molecules), some of the classical continuum transport laws are no longer applicable. It is generally believed that the microscopic description of Boltzmann equation (classical and semiclassical) is adequate to treat transport phenomena in the mesoscale range. Different types of carriers may involve simultaneously in a single problem, therefore, it is desirable to have a method that can allow one to treat them in a unified and parallel manner. Indeed, this is the view advocated in micro- and nano-scale energy transport by Chen [10]. With the semiclassical Boltzmann equation, it is possible to describe adequately the mesoscale transport of particles of arbitrary statistics.

The principal difficulty encountered in solving semiclassical Boltzmann equation as derived by Uehling and Uhlenbeck is the same as that encountered in the classical counterpart and is mainly due to the complicated integral nature of its collision term. The relaxation time approximation proposed by Bhatnagar, Gross and Krook (BGK) [11] for the classical Boltzmann equation provides a much simpler form of collision term and retains the principal effects of particle collisions and enables more tractable solution methods. The BGK relaxation time concept is rather general and can be applicable to the semiclassical Boltzmann

equation as well. The only change is that the equilibrium Maxwell-Boltzmann distribution in the classical case is replaced by the Bose-Einstein or Fermi-Dirac distribution depending on the types of carrier particles. The semiclassical Boltzmann-BGK equation has been widely applied for electron carrier transport in semiconductor, see [12], [13], [14], [15], [16], [17], [18], [19], [20] and phonon energy transport in thermoelectric materials [10]. Similarly, the solution methodology developed for classical Boltzmann-BGK equation can be applied to the semiclassical Boltzmann-BGK equation in phase space. In this work, we aim at developing an accurate direct solver for the semiclassical Boltzmann-BGK equation in phase space that can treat particles of three statistics on equal foot and in a parallel manner. Such a method will allow one to examine the same physical flow problems but with different gas of particles. It is noted that even when solving the problems for the classical Maxwell-Boltzmann statistics, the present formulation allows the analysis of fugacity which has not been included in the original Boltzmann-BGK equation [11] nor in most of other existing works based on it. First, depending on the carrier particles, the discrete ordinate method is used to discretize the velocity (or momentum or wave number) space in the semiclassical Boltzmann-BGK equation into a set of equations for the discrete distribution functions which are continuous in physical space with source terms [21]. Second, the resulting equations can be treated as scalar hyperbolic conservation law with stiff source term whose evolution in space and time can be modeled by existing shock-capturing schemes such as total variation diminishing (TVD) schemes [22] and weighted essentially non-oscillatory (WENO) schemes [23], both of which are adopted in this paper to describe the evolution of these equations.

This paper is organized as follow: Elements of semiclassical Boltzmann-BGK equation is briefly described in Section 2. Its correlation with hydrodynamic equations is outlined. In Section 3, we describe the use of discrete ordinate method to discretize the particle distribution function into a set of hyperbolic conservation laws with source terms. In section 4 we present the description of explicit and implicit time integration formula in capturing the evolution of discretized distribution function equations. In Section 5, numerical experiments of two-dimensional semiclassical gas dynamical flows are presented to illustrate the present algorithm. Finally, concluding remarks will be given in section 6.

2 Semiclassical Boltzmann - BGK Equation

In this section, we delineate the elements of semiclassical Boltzman-BGK equation which we expect to tackle in the present work. Following the works of [2], we consider the extension of the Boltzmann equation to quantum systems due to Uehling and Uhlenbeck in which they took the Pauli exclusion principle into account.

It should be emphasized here that, parallel to classical Boltzmann equation, one can extend the classical to semiclassical formulation. The semiclassical Boltzmann equation (also called Uehling-Uhlenbeck Boltzmann equation) is used to describe the flow for fermions and bosons. The main difference between semiclassical Boltzmann equation and classical Boltzmann equation is the derivation of collision term (right hand side of Boltzmann equation). The collision term is described by time-dependent perturbation theory in quantum mechanics. This generalization is necessary when considering degenerate gases. Since the left hand side of semiclassical Boltzmann equation are the same as classical one, we do not need to repeat it again.

As stated above, the major and only difference between semiclassical Boltzmann equation and classical Boltzmann equation is the collision term. In the classical one, collision term is derived based on classical mechanics [24] while it is derived by quantum scattering theory in the semiclassical one [25]. The collision term for semiclassical Boltzmann equation is described below.

$$\left(\frac{\partial f}{\partial t}+\frac{\mathbf{p}}{m}\cdot\nabla_x-\nabla U(\mathbf{x},t)\cdot\nabla_{\mathbf{p}}\right)f(\mathbf{p},\mathbf{x},t)=\left(\frac{\delta f}{\delta t}\right)_{\text{coll.}} \tag{1}$$

where m is the particle mass, U is the mean field potential and $f(\mathbf{p},\mathbf{x},t)$ is the distribution function which represents the average density of particles with momentum $\mathbf{p}$ at the space-time point $\mathbf{x},t$. The $(\delta f/\delta t)_{coll.}$ denotes the collision term and according to Uehling and Uhlenbeck, it takes the form,

$$\begin{aligned}(\frac{\delta f}{\delta t})^{UU}_{coll.} &= \int d\mathbf{p}\int d\Omega K(\mathbf{p},\mathbf{q},\Omega)\{[1+\theta f(\mathbf{p},t)][1+\theta f(\mathbf{q})]f(\mathbf{p}^*,t)f(\mathbf{q}^*,t)\\ &\quad -[1+\theta f(\mathbf{p}^*,t)][1+\theta f(\mathbf{q}^*)]f(\mathbf{p},t)f(\mathbf{q},t)\},\end{aligned} \tag{2}$$

where $K(\mathbf{p}, \mathbf{q}, \Omega)$ denotes the collision kernel and Ω is the solid angle and θ is a parameter which specifies the type of particle statistics. Here, for $\theta = +1$, Bose-Einstein particles are considered, for $\theta = -1$, Fermi-Dirac particles, and for $\theta = 0$, the Maxwell-Boltzmann classical particles are considered. According to the Boltzmann's H-theorem and conservation conditions, the collision integral of the semiclassical Boltzmann equation will automatically vanish when the distribution functions are in equilibrium and the equilibrium distribution function for general statistics can be expressed as

$$f^{\mathrm{eq}}(\mathbf{p}, \mathbf{x}, t) = \frac{1}{z^{-1} \exp\left\{ [\mathbf{p} - m\,\mathbf{u}(\mathbf{x}, t)]^2 / 2mk_B T(\mathbf{x}, t) \right\} + \theta} \tag{3}$$

where $\mathbf{u}(\mathbf{x}, t)$ is the mean velocity, $T(\mathbf{x}, t)$ is temperature, k_B is the Boltzmann constant and $z(\mathbf{x}, t) = exp\left(\mu(\mathbf{x}, t)/k_B T(\mathbf{x}, t)\right)$ is the fugacity, where μ is the chemical potential. In (3), $\theta = -1$ denotes the Fermi-Dirac statistics, $\theta = +1$, the Bose-Einstein statistics and $\theta = 0$ denotes the Maxwell-Boltzmann statistics. We note that even with the case of $\theta = 0$, we still have chemical potential μ or fugacity z which is rather different from the usual classical Maxwellian distribution.

One of the main functions of the particlle collision term is to drive the gas distribution function f back to equilibrium state f^{eq} corresponding to the local values of number density, momentum density and energy density $n, n\mathbf{u}$ and ϵ. The collision theory assumes that during a time dt, a fraction of dt/τ of molecules in a given small volume undergoes collision, where τ is the average time interval between successive particle collisions for the same particle. The collision term in the BGK model alters the velocity-distribution function from f to f^{eq}. This is equivalent to assuming that the rate of changes df/dt of f due to collisions is $-(f - f^{\mathrm{eq}})/\tau$. Hence, in this dissertation, to avoid the mathematical difficulty caused by the nonlinear integral collision term , the relaxation time concept of Bhatnagar, Gross and Krook is generally applied to replace the collision term of Uehling and Uhlenbeck. Thus the semiclassical Boltzmann-BGK equation reads

$$\left(\frac{\partial f}{\partial t} + \frac{\mathbf{p}}{m} \cdot \nabla_x - \nabla U(\mathbf{x}, t) \cdot \nabla_{\mathbf{p}} \right) f(\mathbf{p}, \mathbf{x}, t) = \left(\frac{\delta f}{\delta t} \right)_{\mathrm{coll.}}^{\mathrm{BGK}} = - \frac{f - f^{\mathrm{eq}}}{\tau} \tag{4}$$

Here, τ is the relaxation time and needs to be specified for each carrier scattering.The model shares the same form with classical BGK equation, but the equilibrium distribution is the semiclassical distribution instead. Hence the system will relax to semiclassical equilibrium distribution instead of classical Maxwellian. Furthermore, in this dissertation, the model is specified as semiclassical Boltzmann-BGK model (SB-BGK) to avoid the ambiguity to classical BGK model. Although the effect of collision is simplified in SB-BGK model, it still retains the main character of collision once the relaxation time is correctly modeled. The collision term in either classical BGK or SB-BGK model should preserve the conservation property.

2.1 Semiclassical Hydrodynamic Equations

Analogous to the classical Boltzmann equation, the Chapman-Enskog procedure has been generalized to obtain the expressions for the transport coefficients such as shear viscosity and thermal conductivity in the hydrodynamic equations. The semiclassical hydrodynamic equations are obtained by taking moments to the semiclassical Boltzmann equation. Theses conservation laws have the same form as their classical counterparts. However, to close the moment expansion at the three moments for hydrodynamics, one must define the other higher moments in terms of the particle number density, momentum density and energy density. The hydrodynamic conservation laws are obtained by multiplying semiclassical Boltzmann equation by $1, ,$ The macroscopic dynamic variables of interest such as number density, momentum density and energy density are low order moments of the distribution function and are defined by:

$$n(\mathbf{x}, t) = \int \frac{d\mathbf{p}}{h^3} f(\mathbf{p}, \mathbf{x}, t), \tag{5}$$

$$\mathbf{j}(\mathbf{x}, t) = \int \frac{d\mathbf{p}}{h^3} \frac{\mathbf{p}}{m} f(\mathbf{p}, \mathbf{x}, t) = n(\mathbf{x}, t)\, \mathbf{u}(\mathbf{x}, t), \tag{6}$$

$$\epsilon(\mathbf{x}, t) = \int \frac{d\mathbf{p}}{h^3} \frac{\mathbf{p}^2}{2m} f(\mathbf{p}, \mathbf{x}, t). \tag{7}$$

where h is Planck's constant. Other higher-order moments such as stress tensor P_{ij} and the heat flux vector $\Phi_i(\mathbf{x},t)$ can also be defined accordingly as

$$P_{ij}(\mathbf{x},t) = \int \frac{d\mathbf{p}}{h^3}(\frac{p_i}{m}-u_i)(\frac{p_j}{m}-u_j)\, f\,(\mathbf{p},\mathbf{x},t), \tag{8}$$

$$\Phi_i(\mathbf{x},t) = \int \frac{d\mathbf{p}}{h^3}\frac{(\mathbf{p}-m\mathbf{u})^2}{2m}(\frac{p_i}{m}-u_i)\, f\,(\mathbf{p},\mathbf{x},t). \tag{9}$$

The conservation laws of macroscopic properties can be obtained by multiplying Eq. (1) respectively by 1, $\mathbf{p}$ and $\mathbf{p}^2/2m$ and integrating the resulting equations over all $\mathbf{p}$. Consequently, the integrals of the collision terms in all three cases vanish automatically resulting in the conservation laws in the form of differential equations for the conserved macroscopic quantities i.e., number density $n(\mathbf{x},t)$, momentum density $mn\mathbf{u}(\mathbf{x},t)$, and energy density $\epsilon(\mathbf{x},t)$ as follow:

$$\frac{\partial n\,(\mathbf{x},t)}{\partial t} + \nabla_x\cdot\mathbf{j}\,(\mathbf{x},t) = 0, \tag{10}$$

$$\frac{\partial m\mathbf{j}\,(\mathbf{x},t)}{\partial t} + \nabla_x\cdot\int\frac{d\mathbf{p}}{h^3}\,\mathbf{p}\,\frac{\mathbf{p}}{m}f\,(\mathbf{p},\mathbf{x},t) = -n(\mathbf{x},t)\nabla_{\mathbf{x}}U(\mathbf{x},t), \tag{11}$$

$$\frac{\partial \epsilon\,(\mathbf{x},t)}{\partial t} + \nabla_x\cdot\int\frac{d\mathbf{p}}{h^3}\,\frac{\mathbf{p}}{m}\,\frac{\mathbf{p}^2}{2m}f\,(\mathbf{p},\mathbf{x},t) = -\mathbf{j}(\mathbf{x},t)\cdot\nabla_{\mathbf{x}}U(\mathbf{x},t). \tag{12}$$

Derivations of the semiclassical Euler and Navier-Stokes equations from the Boltzmann-BGK equation can be obtained from the zeroth order and first order solutions via the Chapman and Enskog expansion [1]. Also, the transport coefficients such as the viscosity η and the thermal conductivity κ can be derived in terms of the relaxation time as

$$\eta = \tau n k_B T\frac{\mathcal{Q}_{5/2}(z)}{\mathcal{Q}_{3/2}(z)} \tag{13}$$

and

$$\kappa = \tau\frac{5k_B}{2m}nk_BT[\frac{7}{2}\frac{\mathcal{Q}_{7/2}(z)}{\mathcal{Q}_{3/2}(z)} - \frac{5}{2}\frac{\mathcal{Q}_{5/2}(z)}{\mathcal{Q}_{3/2}(z)}] \tag{14}$$

where $\mathcal{Q}_\nu(z)$ is the Fermi or Bose function of order ν. For similar results derived from the linearized semiclassical Boltzmann equation, see [4]. Here the case of two space dimensions is assumed. The relaxation times for various scattering mechanisms of different carrier transport in semiconductor devices including electrons, holes, phonons and others have been proposed [15].

In this work, we will also consider the case of semiclassical *Euler limit* in which the particle distribution function is always in equilibrium, i.e., $f = f^{\mathrm{eq}}$ and the collision term of Eq. (1) vanishes automatically. In the later section, we will present the comparison of our results with those of the semiclassical Euler solutions. In recent years, notable numerical methods to describe the ideal quantum gas flows have been developed, see [26, 27, 28].

Before we proceed, without losing generality, we neglect the influence of externally applied field $U(\mathbf{x},t)$.

To illustrate the present method, we formulate the equilibrium distribution in two spatial dimension as the following,

$$f^{\mathrm{eq}}\,(p_x,p_y,x,y,t) = \frac{1}{z^{-1}\exp\left((p_x-mu_x)^2+(p_y-mu_y)^2\right)/(2mk_BT(x,y,t))+\theta}. \tag{15}$$

In a closed form in terms of quantum functions, we replace the distribution function f with f^{eq} which automatically reduces the source term in the BGK Boltzmann equation to zero. The macroscopic moments,

i.e., number density $n(x,y,t)$, momentum $j(x,y,t)$ and energy density $\epsilon(x,y,t)$ are given by

$$\begin{aligned} n(x,y,t) &= \int\int \frac{dp_x\, dp_y}{h^2} f^{\mathrm{eq}}(p_x,p_y,x,y,t) \\ &= \frac{\mathcal{Q}_1(z)^2}{\lambda} \end{aligned} \tag{16}$$

$$\begin{aligned} j_x(x,y,t) &= \int\int \frac{dp_x\, dp_y}{h^2} \frac{p_x}{m} f^{\mathrm{eq}}(p_x,p_y,x,y,t) \\ &= n(x,y,t)u_x(x,y,t) \end{aligned} \tag{17}$$

$$\begin{aligned} j_y(x,y,t) &= \int\int \frac{dp_x\, dp_y}{h^2} \frac{p_y}{m} f^{\mathrm{eq}}(p_x,p_y,x,y,t) \\ &= n(x,y,t)u_y(x,y,t) \end{aligned} \tag{18}$$

$$\begin{aligned} \epsilon(x,y,t) &= \int\int \frac{dp_x\, dp_y}{h^2} \frac{{p_x}^2+{p_y}^2}{2m} f^{\mathrm{eq}}(p_x,p_y,x,y,t) \\ &= \frac{\mathcal{Q}_2(z)}{\beta\lambda^2} + \frac{1}{2}mn({u_x}^2+{u_y}^2) \\ &= \frac{P(x,y,t)}{(\gamma+1)} + \frac{1}{2}mn({u_x}^2+{u_y}^2) \end{aligned} \tag{19}$$

where $\lambda = \sqrt{\frac{\beta h^2}{2\pi m}}$ is the thermal wavelength, P is pressure and $\beta = 1/k_B T(x,y,t)$. The functions $\mathcal{Q}_\nu(z)$ of order ν are respectively defined for Fermi-Dirac and Bose-Einstein statistics as

$$\mathcal{F}_\nu(z) \equiv \frac{1}{\Gamma(\nu)} \int_0^\infty dx \frac{x^{\nu-1}}{z^{-1}e^x+1} \approx \sum_{l=1}^{\infty} (-1)^{l-1} \frac{z^l}{l^\nu} \tag{20}$$

$$\mathcal{B}_\nu(z) \equiv \frac{1}{\Gamma(\nu)} \int_0^\infty dx \frac{x^{\nu-1}}{z^{-1}e^x-1} \approx \sum_{l=1}^{\infty} \frac{z^l}{l^\nu} \tag{21}$$

Here, $\mathcal{F}_\nu(z)$ applies for Fermi-Dirac integral and $\mathcal{B}_\nu(z)$ for Bose-Einstein's, whereas $\Gamma(\nu)$ is gamma function. Further details of the numerical application of these functions can be found in the Appendix B. The definition of macroscopic quantities in terms of Fermi or Bose function applies for both cases of quantum distributions. One only needs to replace Fermi function with Bose function or vice versa whilst maintaining the same procedure. In one-spatial dimension, the distribution function for the three statistics can be expressed as

$$f^{\mathrm{eq}}(p_x, x,\ t) = \frac{1}{z^{-1}\, exp\left\{[p_x - mu_x]^2/2mk_BT(x,t)\right\} + \theta} \tag{22}$$

and the hydrodynamic moments are to be obtained respectively through

$$n(x,t) = \int \frac{dp_x}{h} f^{\mathrm{eq}}(p_x,x,t) = \frac{\mathcal{Q}_{1/2}(z)}{\lambda} \tag{23}$$

$$j(x,t) = \int \frac{dp_x}{h} \frac{p_x}{m} f^{\mathrm{eq}}(p_x,x,t) = n(x,t)u_x(x,t) \tag{24}$$

$$\epsilon(x,t) = \int \frac{dp_x}{h} \frac{{p_x}^2}{2m} f^{\mathrm{eq}}(p_x,x,t) = \frac{\mathcal{Q}_{3/2}(z)}{2\beta\lambda} + \frac{1}{2}mnu_x^2 \tag{25}$$

The higher order moments can be similarly calculated, whereas pressure P can be deduced as

$$P(x,t) = nk_BT(x,t)\frac{\mathcal{Q}_{5/2}(z)}{\mathcal{Q}_{3/2}(z)} \tag{26}$$

2.2 Classical limit

Note that for $z \ll 1$, both $\mathcal{Q}_\nu(z)$ functions for all ν behave like z itself, i.e., $\mathcal{Q}_\nu(z) \approx z$. Physically, a large and negative value of chemical potential of a dilute system and high temperature environment do correspond to small z. On the other hand, we know that at the low temperature, the Fermi-Dirac case displays its most distinctive property in terms of one particle per one energy level mapping. We may intuitively say that the hydrodynamic properties of classical case can be acquired by replacing the $\mathcal{Q}_\nu(z)$ function into z itself. In summary, when z approaches zero, the semiclassical distribution function will coincide with its classical counterpart. Another physical explanation is that the length of particle's dimension is larger than the particle's de Broglie wavelength. The wave property would thus be unimportant. When z is considerably large, two length scales become comparable and one cannot omit the semiclassical effect anymore. One may think of fugacity as the index of the degree of degeneracy. The fugacity has some restrictions in two different semiclassical distributions. In the case of Boson, z should not exceed 1 because of the non-negative density, and in the case of Fermion, there are no such restriction on z. Mathematically, we can obtain the classical hydrodynamic properties by applying the same procedure to the Maxwell-Boltzmann statistics as done to the other quantum statistics.

For $\theta = 0$, the distribution function becomes

$$f^{MB}(p_x,p_y,x,y,t) = \frac{1}{\{z^{-1}\,\exp\{[(p_x-mu_x)^2+(p_y-mu_y)^2]/2mk_BT\}\}}. \tag{27}$$

In this case, no approximation for $\mathcal{Q}_\nu(z)$ is required and the macroscopic values for two spatial dimensions can be obtained by

$$n_c(x,y,t) = \int\int \frac{dp_x\,dp_y}{h^2} f^{MB}(p_x,p_y,x,y,t) = \frac{z}{\lambda^2}. \tag{28}$$

In other words, in the classical limit,

$$z(x,y,t) = e^{\mu(x,y,t)/k_BT(x,y,t)} = \lambda^2\, n_c(x,y,t), \tag{29}$$

$$\mu(x,y,t) = k_BT(x,y,t)\ln(\lambda^2\, n_c(x,y,t)). \tag{30}$$

In the later section, we shall see the numerical examples that compare Fermi and Bose gas to the classical limit.

2.3 Normalization

Before proceeding to discretize the equation, in this section we introduce the characteristic properties of V_∞ and t_∞ for the purpose of normalization. The characteristic velocity and time can be defined as,

$$V_\infty = \sqrt{\frac{2k_BT_\infty}{m}}, \qquad t_\infty = \frac{L}{V_\infty}, \tag{31}$$

with L defined as the characteristic length of the problem. Hence the definitions of non-dimensional variables are introduced as

$$\begin{gathered}(\hat{t},\hat{\tau}) = (t,\tau)/t_\infty,\ (\hat{u}_x,\hat{v_x}) = (u_x,v_x)/V_\infty,\ \hat{x} = x/L, \hat{T} = T/T_\infty \\ (\hat{u}_y,\hat{v_y}) = (u_y,v_y)/V_\infty,\ \hat{y} = y/L, \hat{n} = n/\left(\frac{m^2V_\infty^2}{h^2}\right) \\ \hat{j} = j/\left(\frac{m^2V_\infty^3}{h^2}\right),\ \hat{\epsilon} = \epsilon/\left(\frac{m^3V_\infty^4}{h^2}\right),\ \hat{f} = f.\end{gathered} \tag{32}$$

Hence the normalized semiclassical Boltzmann-BGK equation,

$$\frac{\partial \hat{f}(\hat{v}_x, \hat{v}_y, \hat{x}, \hat{y}, \hat{t})}{\partial \hat{t}} + \hat{v}_x \frac{\partial \hat{f}(\hat{v}_x, \hat{v}_y, \hat{x}, \hat{y}, \hat{t})}{\partial \hat{x}} + \hat{v}_y \frac{\partial \hat{f}(\hat{v}_x, \hat{v}_y, \hat{x}, \hat{y}, \hat{t})}{\partial \hat{y}} = -\frac{\hat{f} - \hat{f}^{\mathrm{eq}}}{\hat{\tau}} \tag{33}$$

with $\hat{v}_x$ and $\hat{v}_y$ as particle velocities. Neglecting the *hat* sign, the normalized two-dimensional semiclassical equilibrium distribution function becomes

$$f^{\mathrm{eq}}(v_x, v_y, x, y, t) = \frac{1}{z^{-1} \exp\left((v_x - u_x)^2 + (v_y - u_y)^2\right)/T + \theta} \tag{34}$$

Before the application of discrete ordinate method is described, we shall explain the evolution of the particle distribution function in time. One of the advantages of using BGK model is that it can be solved analytically by following the characteristic line, see [29].

3 Discrete Ordinate Method

In this section, the implementation of discrete ordinate method is explained. examples of previous usages of discrete ordinate method on Boltzmann equation is given. Lastly, the methodology of its application is laid down. As applied by Huang and Giddens [30] and Shizgal [31] to the linearized Boltzmann-BGK equation, the discrete ordinate method represents functions by a set of discrete points that coincide with the evaluation points in a quadrature rule. The method replaces the original functional dependency on the integral variable by a set of functions with N elements of $W_i f(x_i)$ with $i = 1, \ldots, N$. The points x_i are quadrature points and W_i are the corresponding weights of the integration rule

$$\int_a^b W(x) f(x) dx = \sum_{i=1}^{N} W_i f(x_i). \tag{35}$$

The interval $[a, b]$ will be either $[0, \infty]$ or $[-\infty, \infty]$ depending on considered application. Different weighting function $W(x)$ is addressed accordingly. The x_i are the roots of the Nth-order polynomial $R_n(x)$ of the set that satisfy,

$$\int_a^b W(x) R_n(x) R_i(x) dx = \delta_{in} \tag{36}$$

where the set polynomials $R_n(x)$, orthonormal with respect to the weight function $W(x)$ on the interval $[a, b]$, form a complete basis of the $L^2[a, b]$ Hilbert space. The first N of these polynomials form a subspace of this Hilbert space which is isomorphic with the $\mathcal{R}^N$ Euclidian space. It may be shown from the treatment of the integral over the interval $[a, b]$ with the quadrature rule equation 35 that the discrete ordinate representation is equivalent to the truncated polynomial representation of the Nth-order.

It is shown from [32] that, in general, the velocity distribution function f for states removed from equilibrium is proportional to $\exp(-c^2)$ just as it is for equilibrium, that f has finite bounds under the specific precision in the velocity space and tends to zero as c tends to infinity (Here c represents the magnitude of the thermal (peculiar) velocity of the molecule, that is $\mathbf{c} = \upsilon - \mathbf{u}$). That is, the integration of the normalized distribution function over all velocity space should yield unity, and the probability of the molecular velocities far removed from the mean velocity u of the flow is always negligible. Thus, in order to replace the continuous dependency of the molecular velocity distribution technique can be introduced to discretize the finite velocity region removed from u. Consequently, the numerical integration of the macroscopic flow moments of the distribution function f over the velocity space can be adequately performed by the same quadrature rule, with f evaluated at only a few discrete velocity points. The selections of the velocity points and the range of the velocity space in the discrete ordinate method are somewhat dependent on the related problems.

Additionally, this method is beneficial given the fact that in the end, we are not just interested in the distribution function per se but in the macroscopic moments and the evaluations of the macroscopic moments. In regard to classical gas dynamics, the discrete ordinate method has been applied to the classical nonlinear model Boltzmann equations for rarefied flow computations [21].

Although in this paper, a full-range Gauss-Hermite quadrature is utilized, in terms of the symmetric quality of the exponential function $\exp -\upsilon^2$ over the interval $-\infty, \infty$, the Gauss-Hermite half-range quadratures can be extended to evaluate the infinite integral of the velocity distribution function over all the velocity space. The discrete velocity ordinate points and the weights corresponding to Gauss-Hermite quadrature can be obtained using the algorithms described by Huang and Giddens, and Shizgal.

The Gauss-Hermite quadrature rule over the interval $[-\infty, \infty]$ reads,

$$\int_{-\infty}^{\infty} exp(-{\upsilon_x}^2) f(\upsilon_x) d\upsilon_x \approx \sum_{\sigma=1}^{\bar{N}} W_\sigma \, f(\upsilon_\sigma) \tag{37}$$

or

$$\int_{-\infty}^{\infty} exp(-{\upsilon_x}^2)[exp({\upsilon_x}^2) f(\upsilon_x)] d\upsilon_x \approx \sum_{\sigma=1}^{\bar{N}} W_\sigma \, exp({\upsilon_\sigma}^2) \, f(\upsilon_\sigma) \tag{38}$$

The discrete points υ_α and weight W_α, with $\alpha = \sigma, \delta$, are tabulated in the table of the Gauss-Hermite quadrature, see [33] and can be found through

$$W_\sigma = \frac{2^{\bar{N}-1} \bar{N}! \sqrt{\pi}}{\bar{N}^2 [H_{\bar{N}-1}(\upsilon_\sigma)]^2} \tag{39}$$

with l is number of quadrature points and where υ_σ are the roots of the Hermite polynomial $H_{\bar{N}}(\upsilon)$. It is known that when calculating the Hermite polynomial this way, the number of the discrete velocity points is limited, as it is very difficult exactly to solve high-order Hermite polynomial.

One of the advantages of using the modified Gauss-Hermite quadrature formula is its relatively high accuracy, but for high freestream temperature or Mach number flows, the number of discrete velocity grid points needed to cover the appropriate velocity range could become quite large. To simulate hypersonic flows, the composite integration method based on equally spaced Newton-Cotes formulas which can be developed by setting the polynomial in the discrete ordinate method as a quadratic interpolating polynomial and the Gauss-Legendre numerical quadrature rule whose integral nodes are determined by using the roots of the kth Legendre polynomials have been applied to this study.

3.1 Application of Discrete Ordinate Method

In two dimensional space, the Gauss-Hermite quadrature rule reads

$$\int_{-\infty}^{\infty} \int_{-\infty}^{\infty} e^{-{\upsilon_x}^2} e^{-{\upsilon_y}^2} f(\upsilon_x, \upsilon_y) d\upsilon_x \, d\upsilon_y \approx \sum_{\sigma=-N_1}^{N_1} \sum_{\delta=-N_2}^{N_2} W_\sigma \, W_\delta \, f_{\sigma,\delta} \tag{40}$$

or

$$\int_{-\infty}^{\infty} \int_{-\infty}^{\infty} e^{-{\upsilon_x}^2} e^{-{\upsilon_y}^2} [e^{{\upsilon_x}^2} e^{{\upsilon_y}^2} f(\upsilon_x, \upsilon_y) d\upsilon_x \, d\upsilon_y] \approx \sum_{\sigma=-N_1}^{N_1} \sum_{\delta=-N_2}^{N_2} W_\sigma \, W_\delta \, e^{{\upsilon_\sigma}^2} e^{{\upsilon_\delta}^2} f_{\sigma,\delta} \tag{41}$$

By applying the discrete ordinate method to the equation (33), the distribution function in phase space $f(\upsilon_x, \upsilon_y, x, y, t)$ can be rendered into a set of hyperbolic conservation equation with source terms for $f_{\sigma,\delta}(x, y, t)$ in the physical space, where $\sigma = -N_1, \ldots, -1, 1, \ldots, N_1$ and $\delta = -N_2, \ldots, -1, 1, \ldots, N_2$. The resulting equations are a set of

$$\frac{\partial f_{\sigma,\delta}(x,y,t)}{\partial t} + \upsilon_\sigma \frac{\partial f_{\sigma,\delta}(x,y,t)}{\partial x} + \upsilon_\delta \frac{\partial f_{\sigma,\delta}(x,y,t)}{\partial y} = - \frac{f_{\sigma,\delta} - {f_{\sigma,\delta}}^{\mathrm{eq}}}{\tau} \tag{42}$$

with $f_{\sigma,\delta}$, υ_σ and υ_δ represent the values of respectively f, υ_x and υ_y evaluated at the discrete velocity points σ and δ.

Once the discrete velocity distribution functions $f_{\sigma,\delta}$ are solved, the macroscopic flow moments at any time in each point of the physical space can be obtained and updated by the appropriate discrete velocity

quadrature method as describe in the following:

$$\begin{aligned} n(x,y,t) &= \int_{-\infty}^{\infty} [f(\upsilon_x,\upsilon_y,x,y,t)e^{{\upsilon_x}^2}\, e^{{\upsilon_y}^2}]e^{-{\upsilon_x}^2}e^{-{\upsilon_y}^2}d\upsilon_x d\upsilon_y \\ &= \sum_{\sigma=-N_1}^{N_1}\sum_{\delta=-N_2}^{N_2} W_\sigma\, W_\delta\, e^{{\upsilon_\sigma}^2}e^{{\upsilon_\delta}^2} f_{\sigma,\delta} \end{aligned} \tag{43}$$

$$\begin{aligned} j_x(x,y,t) &= \int_{-\infty}^{\infty} [\upsilon_x\, f(\upsilon_x,\upsilon_y,x,y,t)e^{{\upsilon_x}^2}\, e^{{\upsilon_y}^2}]e^{-{\upsilon_x}^2}e^{-{\upsilon_y}^2}d\upsilon_x d\upsilon_y \\ &= \sum_{\sigma=-N_1}^{N_1}\sum_{\delta=-N_2}^{N_2} \upsilon_\sigma\, W_\sigma\, W_\delta\, e^{{\upsilon_\sigma}^2}e^{{\upsilon_\delta}^2} f_{\sigma,\delta} \\ &= n(x,y,t)\, u_x(x,y,t) \end{aligned} \tag{44}$$

$$\begin{aligned} j_y(x,y,t) &= \int_{-\infty}^{\infty} [\upsilon_y\, f(\upsilon_x,\upsilon_y,x,y,t)e^{{\upsilon_x}^2}\, e^{{\upsilon_y}^2}]e^{-{\upsilon_x}^2}e^{-{\upsilon_y}^2}d\upsilon_x d\upsilon_y \\ &= \sum_{\sigma=-N_1}^{N_1}\sum_{\delta=-N_2}^{N_2} \upsilon_\delta\, W_\sigma\, W_\delta\, e^{{\upsilon_\sigma}^2}e^{{\upsilon_\delta}^2} f_{\sigma,\delta} \\ &= n(x,y,t)\, u_y(x,y,t) \end{aligned} \tag{45}$$

$$\begin{aligned} \epsilon(x,y,t) &= \int_{-\infty}^{\infty} [\frac{\upsilon_x^2+\upsilon_y^2}{2}\, f(\upsilon_x,\upsilon_y,x,y,t)e^{{\upsilon_x}^2}\, e^{{\upsilon_y}^2}]e^{-{\upsilon_x}^2}e^{-{\upsilon_y}^2}d\upsilon_x d\upsilon_y \\ &= \sum_{\sigma=-N_1}^{N_1}\sum_{\delta=-N_2}^{N_2} (\frac{\upsilon_\sigma^2+\upsilon_\delta^2}{2}) W_\sigma\, W_\delta\, e^{{\upsilon_\sigma}^2}e^{{\upsilon_\delta}^2} f_{\sigma,\delta} \end{aligned} \tag{46}$$

Pressure $P(x,y,t)$ can be defined as

$$P(x,y,t) = [\epsilon(x,y,t) - \frac{1}{2}n(x,y,t)(u_x^2+u_y^2)](\gamma-1) \tag{47}$$

The value of relaxation time is given by

$$\tau = \eta/P \tag{48}$$

Of course, for one dimensional case, the macroscopic quantities can be obtained similarly e.g., the density can be calculated as

$$\begin{aligned} n(x,t) &= \int_{-\infty}^{\infty} [f(\upsilon_x,x,t)e^{{\upsilon_x}^2}]e^{-{\upsilon_x}^2}d\upsilon_x \\ &\approx \sum_{\sigma=1}^{\bar{N}} W_\sigma\, [f_\sigma\, e^{{\upsilon_\sigma}^2}] \end{aligned} \tag{49}$$

which can be analogously defined for the composite Boole's rule as a class of Newton-Cotes quadratures, for

example

$$\begin{aligned} n(x,t) &= \int_{-\infty}^{\infty} f(\upsilon_x, x, t) d\upsilon_x \\ &\approx h \sum_{\sigma=1}^{\bar{N}} H_\sigma f_\sigma(x,t). \end{aligned} \tag{50}$$

Here, we note that the basic criteria of choosing different quadratures is to guarantee that the macroscopic moments can be accurately computed which requiring the accurate representation of the distribution function with suitable velocity range being covered. The equally spaced Newton-Cotes formula can also be used if one needs to cover the high energy tail of the distribution function.

4 Numerical Method

On Cartesian grid, the explicit and implicit methods of the current work is developed. This section of the paper will elaborate the application of both methods. To begin, we firstly discretize the space x, y and time t into a number of cells centered at i, j at time n, hence we approximate $f_{\sigma,\delta}$ by ${f_{\sigma,\delta}}_{i,j}^{n}$. First, In terms of numerical fluxes and in explicit first order accurate in time and fully discrete form, the evolution from n^{th} time level to $(n+1)^{th}$ time level is expressed by

$$\begin{aligned} {f_{\sigma,\delta}}_{i,j}^{n+1} &= {f_{\sigma,\delta}}_{i,j}^{n} - \frac{\Delta t}{\Delta x}\left(F^N_{i+1/2,j} - F^N_{i-1/2,j}\right) \\ &- \frac{\Delta t}{\Delta y}\left(G^N_{i,j+1/2} - G^N_{i,j-1/2}\right) + \frac{\Delta t}{\tau}\left({f^{eq}_{\sigma,\delta}}_{i,j}^{\,n} - {f_{\sigma,\delta}}_{i,j}^{n}\right) \end{aligned} \tag{51}$$

From this point further description of the numerical flux $F^N_{i+1/2,j}$ can be given according to specific numerical methods.

4.1 Implementation of WENO

The representation of numerical fluxes in Eqs. 51 according to WENO schemes is given as follows

$$F^N_{i+1/2,j} = F^+_{i+1/2,j} + F^-_{i+1/2,j}\,,\; G^N_{i,j+1/2} = G^+_{i,j+1/2} + G^-_{i,j+1/2} \tag{52}$$

where the split flux vectors are defined by

$$\begin{aligned} F^+_{i,j} &= \upsilon^+_\sigma f_{\sigma,\delta_{i,j}}\,, \quad F^-_{i,j} = \upsilon^-_\sigma f_{\sigma,\delta_{i,j}} \\ G^+_{i,j} &= \upsilon^+_\delta f_{\sigma,\delta_{i,j}}\,, \quad G^-_{i,j} = \upsilon^-_\delta f_{\sigma,\delta_{i,j}} \end{aligned} \tag{53}$$

Here, $\upsilon^\pm_\sigma = (\upsilon_\sigma \pm |\upsilon_\sigma|)/2$ and $\upsilon^\pm_\delta = (\upsilon_\delta \pm |\upsilon_\delta|)/2$. Numerical fluxes for the positive part are expressed as

$$\begin{aligned} F^+_{i+1/2,j} &= \omega^+_0\left(\frac{2}{6}F^+_{i-2,j} - \frac{7}{6}F^+_{i-1,j} + \frac{11}{6}F^+_{i,j}\right) \\ &+ \omega^+_1\left(-\frac{1}{6}F^+_{i-1,j} + \frac{5}{6}F^+_{i,j} + \frac{2}{6}F^+_{i+1,j}\right) \\ &+ \omega^+_2\left(\frac{2}{6}F^+_{i,j} + \frac{5}{6}F^+_{i+1,j} - \frac{1}{6}F^+_{i+2,j}\right) \end{aligned} \tag{54}$$

$$\omega^+_k = \frac{\alpha^+_k}{\alpha^+_0 + \alpha^+_1 + \alpha^+_2}\,, \quad k = 0, 1, 2 \tag{55}$$

$$\alpha_0^+ = \frac{1}{10(\epsilon + IS_0^+)^2},\ \alpha_1^+ = \frac{6}{10(\epsilon + IS_1^+)^2},\ \alpha_2^+ = \frac{3}{10(\epsilon + IS_2^+)^2} \tag{56}$$

$$\begin{aligned} IS_0^+ &= \frac{13}{12}\left(F_{i-2,j}^+ - 2F_{i-1,j}^+ + F_{i,j}^+\right)^2 + \frac{1}{4}\left(F_{i-2,j}^+ - 4F_{i-1,j}^+ + 3F_{i,j}^+\right)^2 \\ IS_1^+ &= \frac{13}{12}\left(F_{i-1,j}^+ - 2F_{i,j}^+ + F_{i+1,j}^+\right)^2 + \frac{1}{4}\left(F_{i-1,j}^+ - F_{i+1,j}^+\right)^2 \\ IS_2^+ &= \frac{13}{12}\left(F_{i,j}^+ - 2F_{i+1,j}^+ + F_{i+2,j}^+\right)^2 + \frac{1}{4}\left(3F_{i,j}^+ - 4F_{i+1,j}^+ + F_{i+2,j}^+\right)^2 \end{aligned} \tag{57}$$

Whereas the numerical flux for the negative part is given by

$$\begin{aligned} F_{i+1/2,j}^- &= \omega_0^-\left(-\frac{1}{6}F_{i-1,j}^- + \frac{5}{6}F_{i,j}^- + \frac{2}{6}F_{i+1,j}^-\right) \\ &+ \omega_1^-\left(\frac{2}{6}F_{i,j}^- + \frac{5}{6}F_{i+1,j}^- - \frac{1}{6}F_{i+2,j}^-\right) \\ &+ \omega_2^-\left(\frac{11}{6}F_{i+1,j}^- - \frac{7}{6}F_{i+2,j}^- + \frac{2}{6}F_{i+3,j}^-\right) \end{aligned} \tag{58}$$

$$\omega_k^- = \frac{\alpha_k^-}{\alpha_0^- + \alpha_1^- + \alpha_2^-},\quad k = 0, 1, 2 \tag{59}$$

$$\alpha_0^- = \frac{3}{10(\epsilon + IS_0^-)^2},\ \alpha_1^- = \frac{6}{10(\epsilon + IS_1^-)^2},\ \alpha_2^- = \frac{1}{10(\epsilon + IS_2^-)^2} \tag{60}$$

$$\begin{aligned} IS_0^- &= \frac{13}{12}\left(F_{i-1,j}^- - 2F_{i,j}^- + F_{i+1,j}^-\right)^2 + \frac{1}{4}\left(F_{i-1,j}^- - 4F_{i,j}^- + 3F_{i+1,j}^-\right)^2 \\ IS_1^- &= \frac{13}{12}\left(F_{i,j}^- - 2F_{i+1,j}^- + F_{i+2,j}^-\right)^2 + \frac{1}{4}\left(F_{i,j}^- - F_{i+2,j}^-\right)^2 \\ IS_2^- &= \frac{13}{12}\left(F_{i+1,j}^- - 2F_{i+2,j}^- + F_{i+3,j}^-\right)^2 \\ &+ \frac{1}{4}\left(3F_{i+1,j}^- - 4F_{i+2,j}^- + F_{i+3,j}^-\right)^2 \end{aligned} \tag{61}$$

The expression of $G_{i,j+1/2}^+$ and $G_{i,j+1/2}^-$ for y direction can be derived in a similar fashion.

4.2 Implementation of TVD

For comparison purpose, we also implement a second-order TVD scheme [22]. TVD scheme with particularly Van Leer's limiter [34] is utilized in this work. The scheme is of second-order accurate and aside for the purpose of comparison, the inclusion of TVD scheme is to appeal to CFD practitioners with less computational resources. TVD scheme requires different and rather simpler treatment of boundary condition. Although its spatial accuracy is not as high as that of WENO, second-order accurate numerical schemes may be adequate for engineers who use this method in more practical implementations and who seek quicker results without emphasizing much on excellent accuracy. In other words, it may serve as a reliable substitute which demands less computational power and memory.

Using the same expression as Eq. (51), we can also define the numerical fluxes for a TVD scheme given by

$$\begin{aligned} F_{i+1/2,j}^N &= \mathcal{F}_L(f_{\sigma,\delta_{i,j}}, f_{\sigma,\delta_{i+1,j}}) + \phi(\theta_{xi+1/2,j})[\mathcal{F}_H(f_{\sigma,\delta_{i,j}}, f_{\sigma,\delta_{i+1,j}}) \\ &- \mathcal{F}_L(f_{\sigma,\delta_{i,j}}, f_{\sigma,\delta_{i+1,j}})] \end{aligned} \tag{62}$$

where $\mathcal{F}_L(f_{\sigma,\delta_{i,j}}, f_{\sigma,\delta_{i+1,j}})$ are the low order upwind flux given by

$$\mathcal{F}_L(f_{\sigma,\delta_{i,j}}, f_{\sigma,\delta_{i+1,j}}) = \upsilon_\sigma^+ f_{\sigma,\delta_{i,j}} + \upsilon_\sigma^- f_{\sigma,\delta_{i+1,j}}, \tag{63}$$

with the high order Lax-Wendroff scheme given by

$$\begin{aligned} \mathcal{F}_H(f_{\sigma,\delta_{i,j}}, f_{\sigma,\delta_{i+1,j}}) &= (\upsilon_\sigma^+ f_{\sigma,\delta_{i,j}} + \upsilon_\sigma^- f_{\sigma,\delta_{i+1,j}}) \\ &+ \frac{1}{2}|\upsilon_\sigma|\left(1 - \frac{\Delta t}{\Delta x}|\upsilon_\sigma|\right)(f_{\sigma,\delta_{i+1,j}} - f_{\sigma,\delta_{i,j}}). \end{aligned} \tag{64}$$

Here, $\upsilon_\sigma^\pm = (\upsilon_\sigma \pm |\upsilon_\sigma|)/2$ and similarly, $\upsilon_\delta^\pm = (\upsilon_\delta \pm |\upsilon_\delta|)/2$; whereas for the limiter function $\phi(\theta_{xi+1/2,j})$, Van Leer's limiter is chosen and is given by

$$\begin{aligned} \phi(\theta_{xi+1/2,j}) &= \frac{(|\theta_{xi+1/2,j}| + \theta_{xi+1/2,j})}{1 + |\theta_{xi+1/2,j}|} \\ \theta_{xi+1/2,j} &= \frac{f_{\sigma,\delta}{}^n_{i'+1,j} - f_{\sigma,\delta}{}^n_{i',j}}{f_{\sigma,\delta}{}^n_{i+1,j} - f_{\sigma,\delta}{}^n_{i,j}}, \quad i' = i - \mathrm{sgn}\left(\upsilon_\sigma \frac{\Delta t}{\Delta x}\right). \end{aligned} \tag{65}$$

The application of WENO and TVD which are respectively fifth and second order accurate entails differing treatment of boundary condition considering the nature of these schemes' stencils. The inclusion of these two methods is not intended to subordinate any of these schemes, instead interested readers can choose between these two methods in accordance to the computational resources available.

In order to solve steady state gas flow problems, one usually resort to implicit methods instead of explcit methods. This is due to the fact that explicit method entails the Courant-Friedrich-Lewy condition which limit the time-step rather strictly. The CFL condition requires that the region of dependence of the difference scheme must at least include the region of dependence of the differential equation.

Implicit schemes theoretically lift all the restrictions on numerical time-step due to convection term, hence enable faster convergence rate. Along the developments of implicit schemes, approximate factorizations are commonly embedded with the schemes.

The application of Euler implicit time differencing formula on the current method is reported. More sophisticated higher order accurate (in time) implicit formulas are subject to future endeavor. Here, the emphasis is simply to test the new algorithm on implicit time integration framework.

In this section the implicit numerical algorithm to solve Eq. (42) is delineated. The LU factorization [35] is utilized. Using the Euler implicit time-differencing formula, Eq. (42) can be written as

$$[I + \Delta t(D_x\upsilon_\sigma + D_y\upsilon_\delta + S)]\Delta f_{\sigma,\delta}{}^{(n+1)}_{i,j} = RHS^n_{i,j} \tag{66}$$

where $\Delta f_{\sigma,\delta}{}^{(n+1)}_{i,j} = f_{\sigma,\delta}{}^{(n+1)}_{i,j} - f_{\sigma,\delta}{}^{(n)}_{i,j}$, I is the unit matrix, $S = \frac{\partial(f_{\sigma,\delta} - f^{eq}_{\sigma,\delta}/\tau)}{\partial f_{\sigma,\delta}}$. The time step Δt is chosen to be less than the local relaxation time, τ. $RHS^n_{i,j}$ is defined as

$$RHS^n_{i,j} = -\Delta t\left(\upsilon_\sigma \frac{\partial f_{\sigma,\delta}}{\partial x} + \upsilon_\delta \frac{\partial f_{\sigma,\delta}}{\partial y} + \frac{f_{\sigma,\delta} - f_{\sigma,\delta}{}^{eq}}{\tau}\right)^n_{i,j} \tag{67}$$

Applying the lower-upper factorization method to Eq. (66) we achieve

$$[I + \Delta t(L + U + S)]\Delta f_{\sigma,\delta}{}^{(n+1)}_{i,j} = RHS^n_{i,j} \tag{68}$$

where

$$\begin{aligned} L &= D_x^-\upsilon_\sigma^+ + D_y^-\upsilon_\delta^+, \qquad U = D_x^+\upsilon_\sigma^- + D_y^+\upsilon_\delta^- \\ RHS^n_{i,j} &= -\frac{\Delta t}{\Delta x}\left(F^N_{i+1/2,j} - F^N_{i-1/2,j}\right) - \frac{\Delta t}{\Delta y}\left(G^N_{i,j+1/2} - G^N_{i,j-1/2}\right) \\ &+ \frac{\Delta t}{\tau}\left(f^{eq\,n}_{\sigma,\delta_{i,j}} - f_{\sigma,\delta}{}^n_{i,j}\right) \end{aligned} \tag{69}$$

Here, D^- and D^+ denote the backward and forward difference operators respectively. Although in theory, implicit method is utilized such that the chosen time-step can be larger, the fact that the linearization is done in terms of first order accurate backward and forward difference method, eventually limits the time-step. We chose the first-order linearization because TVD or WENO schemes are highly non-linear and it would take a huge computational resource to do so. Hence, the discrepancy between the spatial discretization and its Jacobian's order of accuracy contributes to the limitation of time-step [36]. $\upsilon^{\pm}_{\sigma,\delta} = (\upsilon_{\sigma,\delta} \pm |\upsilon_{\sigma,\delta}|)/2$, whereas F and G are the numerical fluxes which will be described in the following section.

The approximate LU factorization can be given as

$$[E + \Delta t L]E^{-1}[E + \Delta t U]\Delta {f_{\sigma,\delta}}_{i,j}^{(n+1)} = RHS_{i,j}^{n}, \qquad E = I + \Delta t S \tag{70}$$

which can be sequentially solved by:

$$[E + \Delta t L]\Delta {f_{\sigma,\delta}}_{i,j}^{*} = RHS_{i,j}^{n}, \tag{71}$$

$$[E + \Delta t U]\Delta {f_{\sigma,\delta}}_{i,j}^{(n+1)} = \Delta {f_{\sigma,\delta}}_{i,j}^{*}, \tag{72}$$

and lastly,

$${f_{\sigma,\delta}}_{i,j}^{(n+1)} = {f_{\sigma,\delta}}_{i,j}^{(n)} + \Delta {f_{\sigma,\delta}}_{i,j}^{(n+1)}, \tag{73}$$

The approximation factorization error of Eq. 70 can be calculated as

$$E_{LU} = \Delta t^2 L E^{-1} U \Delta {f_{\sigma,\delta}}_{i,j}^{n+1} \tag{74}$$

which can be shown to produce the least amount of error among several possible factorizations, particularly when the norms of the source terms are large [37].

5 Computational Experiments

In this section, several computational experiments are done to demonstrate the ability of the developed solver. Both transient and steady state problems are considered. A range of relaxation times and Knudsen numbers are tested to illustrate flows in near continuum and transitional regimes. Firstly, we define the Knudsen number based on the relation $Kn = \lambda_\infty / L$ which indicates the degree of rarefaction of the gas flow. Here, the relaxation time will vary with Kn number according to $\tau = \frac{5\sqrt{\pi}\, Kn}{8nT^{(1-\chi)}} \frac{\mathcal{Q}_1(z)}{\mathcal{Q}_2(z)}$, where $\chi = 1$.

A. Numerical simulations on transient problems

In this example, we would like to illustrate the ability of the method in dealing with complex flow field which usually emerges from shock interactions. In this example, WENO is utilized for solving internal flow problems. A square cylinder is placed as an obstacle inside a 2-D narrow duct/channel.

We consider an incident moving shock wave which is located in front and to the left of a square cylinder initially and start to move to the right and impinge upon the square cylinder and encounter the complex shock diffraction processes. The initial condition at state 1(ahead of moving shock) and state 2(behind the moving shock) for the incident shock wave shall obey the Rankine-Hugoniot condition i.e.,

$$\frac{P_2}{P_1} = \frac{2\gamma M_s^2 - (\gamma - 1)}{\gamma + 1} \tag{75}$$

$$\frac{n_2}{n_1} = \frac{G(P_2/P_1) + 1}{G + (P_2/P_1)} \tag{76}$$

$$u_2 = M_s \left[1 - \frac{(\gamma - 1)M_s^2 + 2}{(\gamma + 1)M_s^2}\right] c_1, \tag{77}$$

where $G = (\gamma + 1)/(\gamma - 1)$, M_s is the incident shock Mach number and $c = (\gamma P/n)^{1/2}$ is the local sound speed. For two dimensional case, we utilize $\gamma = 2$.

The boundary condition needs to relate the distribution function of the incoming particle f_I and that of the outgoing particle from the wall f_O. When the specularly reflecting wall is considered, it is assumed that

a particle does not exchange energy with the wall; the wall is adiabatic and no shear stress acting on the wall. Hence, the outgoing distribution function f_O would follow analogously from the incoming distribution function with accordingly transformed normal velocities $f_I(-\upsilon_n)$ i.e.,

$$f_O = f_I(-\upsilon_n, \vec{x}, t), \qquad \upsilon_n \geq 0 \tag{78}$$

where $\upsilon_n = \vec{v} \cdot \vec{n}$ and $\vec{n}$ is the outward unit normal to the stationary solid surface.

Here, $\Delta x = \Delta y = 0.0307$ are used with 20×20 Gauss-Hermite quadrature points. Physically, we set $M_s = 2.0$ and the initial condition for the Fermi-Dirac gas at rest ahead of shock are set as $(n_1, u_{x1}, u_{y_1}, P_1) = (0.1497, 0, 0, 0.038)$ which correspond to $z_1 = 0.1$ and $T_1 = 0.5$, whereas the condition before the shock are set as $(n_2, u_{x2}, u_{y2}, P_2) = (0.2994, 0.7125, 0, 0.192)$ which correspond to $z_2 = 0.078$. The relaxation time is set as $\tau = 0.0001$ which corresponds to Kn $= 0.000105$. In Fig. 1 the important macroscopic quantities like density, pressure, temperature and fugacity are depicted in good detail which then highlights the high-order accuracy of WENO scheme.

In Fig. 1(a) we can see the density contour in which, the accelerated shock is already disturbed by the incoming shock reflected by the channel wall. The decelerated shock here is accompanied by a few diverging acoustics which come in sequences. These acoustic waves form part of eccentric circles, each of which are connected to decelerated shock at its end, resembling a sound source moving with a sonic speed in a quiescent flow medium. The other ends of the circular waves decay quickly near the far boundary, justifying their name diverging acoustics firstly coined by Chang and Chang [38]. The decelarated shock, on the other hand, penetrates the vortex core to develop a transmitted shock. As decelerated shock moves counterclockwise during its expansion, so does the transmitted shock. Here, one can see transmitted shocks connected from the upper and lower vortices already to form a full-fledged transmitted shock. The complexity of the flow field is increased when the reflected shock wave by the channel wall penetrate the front slip layer which develops another accelerated shock.

In the front of the wall, complex shock, slipstream, and square cylinder wall interaction develop another weaker reflected shock, as well at the tail of the square cylinder. Small terminator actually occurs during this simulation since the incoming shock wave is of relatively strong Mach i.e., $M_s = 2.0$. Note that this simulation includes a small value of relaxation time which then contributes viscosity to the flow. Hence, one shall not expect an inviscid-like details as what would be exhibited from solving Euler limit solution.

In Fig. 1(d) the fugacity contour is given. Note that for Maxwell-Boltzmann gas we can also give the analysis of fugacity and chemical potential if desired which is not the case when other contemporary classical gas schemes are considered.

B. Numerical simulations on steady state problems

For solving steady state problems, CFD practicioners commonly resort to implicit scheme due to its ability to relax the time-step limitation imposed by the usage of explicit schemes. Now we would like to demonstrate the ability of the current scheme in solving the steady state problems. The problems chosen is a supersonic flow of gases of arbitrary statistics over a square cylindrical obstacle.

For the first test, we condition the supersonic flow of Mach number $M_\infty = 2.0$ of Fermi-Dirac gas at $n_\infty = 0.2$ and $P_\infty = 0.1$ on Cartesian grids. This corresponds to fugacity $z = 0.0668$. The speed of sound is determined as $c = (\gamma P/n)^{1/2}$, where the gas constant $\gamma = 2$ is taken. A flow near continuum regime is conditioned as small relaxation time of $\tau = 0.0005$ which corresponds to Kn $= 0.000511$ is considered. Numerically, the problem is solved on Cartesian grid using 143×319 grid points. Second order accurate TVD scheme is used along with the Van Leer's limiter [22, 34].

In Fig. 2, the steady state profile of Fermi-Dirac gas is presented. The contours of density, pressure, fugacity and Mach number are plotted. The flow structures including the bow shock, the stagnation region, the near wake, recompression shock, and far wake regions are well captured. In this example, by setting a small relaxation time, the freestream is in the near continuum flow regime and a recirculation zone is present in the near wake region. The enlarged view of this region is well captured in Fig. 3. The history of L_2 norm of residual is plotted. The residual lower than 10^{-7} is taken as our criteria of convergence and can be achieved after approximately 4500 iterations.

In the second test, we consider the supersonic flow of Bose-Einstein gas with the same macroscopic conditioning as used in the first test. Except for different application of relaxation times, other numerical properties in the setup of the problem is the same with that of the first test. Here, we would like to test

the current scheme's ability in tackling big relaxation time which corresponds to the environment close to *transitional regime*. In Figs. 4, the density contour of Bose-Einstein gas at $\tau = 0.1$ (b) is compared to that of the Euler limit solution (a) which can be achieved when the distribution function is assumed to be always at equlibrium. The result of that of Euler limit gives much sharper flow structure compared to that with big relaxation time.

At large relaxation time (and Knudsen number) the thickening of the front bow shock and no recompression shock above the near wake are noticeable differences in more rarefied cases of gas flows when compared to the small relaxation time counterpart.

6 Concluding Remarks

In this work, the explicit and implicit time integration schemes for solving rarefied flow problems of gases of arbitrary statistics based on semiclassical Boltzmann-BGK equation have been presented. Here, the unsteady shock wave diffraction patterns by a square cylinder in gases of particles of arbitrary statistics and a steady supersonic flow of gases of arbitrary statistics over a square cylindrical obstacle are computed by using the accurate solver in phase space. A series of diffraction patterns of different flow properties at various time instants are recorded for detailed flow fields analysis. The numerical method is a combination of the discrete ordinate method and high order methods such as WENO and TVD. Different range of relaxation times and Knudsen numbers covering continuum and rarefied flow regimes are computed. For comparison purpose, the equilibrium limit solution, i.e., zero relaxation time and $f = f^{\text{eq}}$ everywhere, is also computed. The effects of gas particles that obey the Maxwell-Boltzmann, Bose-Einstein and Fermi-Dirac statistics are examined and depicted. When the relaxation time and Knudsen values are small such that the flows are in the continuum regime, all the expected flow features of gas dynamics comprising incident shocks, reflected shocks, triple Mach shocks, slip lines and their roll-up to form vortices can be seen with considerably good detail and are in good agreement with available experimental observations. Moreover, even for gases with Maxwell-Boltzmann statistics, the present results are quite different from traditional classical results as the fugacity or chemical potential is present. The capability in describing the gas flows of arbitrary particle statistics in various flow regimes on equal footing have been illustrated without much major constraints. We believe the present work is the first result that gas dynamical characteristics of three particle statistics in an identical flow problem have been simultaneously exhibited. The present work emphasizes on building the unified and parallel framework for treating semiclassical rarefied gas flows and specific application to different individual carrier in specific physical problem can be separately pursued such as electrons transport [14, 15] and phonon energy transport [39].

References

[1] S. Chapman and T. G. Cowling. *The mathematical theory of non-uniform gases: an account of the kinetic theory of viscosity, thermal conduction, and diffusion in gases.* Cambridge University Press, 1970.

[2] L. P. Kadanoff and G. Baym. *Quantum Statistical Mechanics.* Benjamin, New York, 1962.

[3] E. A. Uehling and G. E. Uhlenbeck. Transport phenomena in einstein-bose and fermi-dirac gases. i. *Phys. Rev.*, 43(7):552–561, Apr 1933.

[4] T. Nikuni and A. Griffin. Hydrodynamic damping in trapped bose gases. *Journal of Low Temperature Physics*, 111:793–814, 1998.

[5] E. Wigner. On the quantum correction for thermodynamic equilibrium. *Phys. Rev.*, 40(5):749–759, Jun 1932.

[6] M. G. Ancona and H. F. Tiersten. Macroscopic physics of the silicon inversion layer. *Phys. Rev. B*, 35(15):7959–7965, May 1987.

[7] Carl L. Gardner. The quantum hydrodynamic model for semiconductor devices. *SIAM J. Appl. Math.*, 54(2):409–427, 1994.

[8] M. G. Ancona and G. J. Iafrate. Quantum correction to the equation of state of an electron gas in a semiconductor. *Phys. Rev. B*, 39(13):9536–9540, May 1989.

[9] D. L. Woolard, H. Tian, M. A. Littlejohn, K. W. Kim, R. J. Trew, M. K. Ieong, and T. W. Tang. Construction of higher-moment terms in the hydrodynamic electron transport model. *Journal of Applied Physics*, 74(10):6197 –6207, nov 1993.

[10] Gang Chen. *Nanoscale Energy Transport and Conversion: A Parallel Treatment of Electrons, Molecules, Phonons, and Photons (Mit-Pappalardo Series in Mechanical Engineering)*. Oxford University Press, USA, March 2005.

[11] P. L. Bhatnagar, E. P. Gross, and M. Krook. A model for collision processes in gases. i. small amplitude processes in charged and neutral one-component systems. *Phys. Rev.*, 94(3):511–525, May 1954.

[12] Mark Lundstrom. *Fundamentals of Carrier Transport*. Cambridge University Press, 2nd edition, 2000.

[13] Emad Fatemi and Faroukh Odeh. Upwind finite difference solution of boltzmann equation applied to electron transport in semiconductor devices. *Journal of Computational Physics*, 108(2):209 – 217, 1993.

[14] Jose A. Carrillo, Irene M. Gamba, Armando Majorana, and Chi-Wang Shu. A weno-solver for the transients of boltzmann-poisson system for semiconductor devices: performance and comparisons with monte carlo methods. *Journal of Computational Physics*, 184(2):498 – 525, 2003.

[15] A. Majorana and R. M. Pidatella. A finite difference scheme solving the boltzmann-poisson system for semiconductor devices: Volume 174, number 2 (2001), pages 649-668. *Journal of Computational Physics*, 177(2):450 – 450, 2002.

[16] Jose A. Carrillo, Irene M. Gamba, Armando Majorana, and Chi-Wang Shu. A weno-solver for the 1d non-stationary boltzmann-poisson system for semiconductor devices. *Journal of Computational Electronics*, 1:365–370, 2002.

[17] Jose A. Carrillo, Irene M. Gamba, Armando Majorana, and Chi-Wang Shu. A direct solver for 2d non-stationary boltzmann-poisson systems for semiconductor devices: A mesfet simulation by weno-boltzmann schemes. *Journal of Computational Electronics*, 2:375–380, 2003.

[18] Peter A. Markowich, Christian A. Ringhofer, and Christian Schmeiser. *Semiconductor Equations*. Springer, 1 edition, 2002.

[19] A. Pattamatta and C. K. Madnia. Modeling electron-phonon nonequilibrium in gold films using boltzmann transport model. *Journal of Heat Transfer*, 131:082401–1, 2009.

[20] S. Scaldaferri, G. Curatola, and G. Iannaccone. Direct solution of the boltzmann transport equation and poisson schrodinger equation for nanoscale mosfets. *IEEE Transaction on Electron Devices*, 54:2901, 2007.

[21] J. Y. Yang and J. C. Huang. Rarefied flow computations using nonlinear model boltzmann equations. *Journal of Computational Physics*, 120(2):323 – 339, 1995.

[22] Ami Harten. High resolution schemes for hyperbolic conservation laws. *Journal of Computational Physics*, 49(3):357 – 393, 1983.

[23] Zhengfu Xu and Chi-Wang Shu. Anti-diffusive flux corrections for high order finite difference weno schemes. *Journal of Computational Physics*, 205(2):458 – 485, 2005.

[24] G. A. Bird. *Molecular gas dynamics and the direct simulation of gas flows*. Oxford University Press, Oxford, 1994.

[25] T. Nikuni and A. Griffin. Hydrodynamic damping in trapped bose gases. *Journal of Low Temperature Physics*, 111(5):793–814, Jun 1998.

[26] J. Y. Yang, T.Y. Hsieh, and Y. H. Shi. Kinetic flux vector splitting schemes for ideal quantum gas dynamics. *SIAM J. Sci. Comput.*, 29(1):221–244, 2007.

[27] Yu Hsin Shi and Jaw Yen Yang. A gas kinetic bgk scheme for semiclassical boltzmann hydrodynamic transport. *Journal of Computational Physics*, 227(22):9389 – 9407, 2008.

[28] Jaw Yen Yang and Yu Hsin Shi. A kinetic beam scheme for ideal quantum gas dynamics. *Proceedings of the Royal Society A: Mathematical, Physical and Engineering Science*, 462(2069):1553–1572, 2006.

[29] Kevin H. Prendergast and Kun Xu. Numerical hydrodynamics from gas-kinetic theory. *Journal of Computational Physics*, 109(1):53 – 66, 1993.

[30] A. B. Huang and D. P. Giddens. The Discrete Ordinate Method for the Linearized Boundary Value Problems in Kinetic Theory of Gases. In C. L. Brundin, editor, *Rarefied Gas Dynamics, Volume 1*, pages 481–+, 1967.

[31] B. Shizgal. A gaussian quadrature procedure for use in the solution of the boltzmann equation and related problems. *Journal of Computational Physics*, 41(2):309 – 328, 1981.

[32] G. H. Findenegg. P.c.riedi: Thermal physics. macmillan press, london 1976. 318 seiten. *Berichte der*

Bunsengesellschaft for physikalische Chemie, 81(2):249–249, 1977.

[33] Milton Abramowitz and Irene A. Stegun. *Handbook of Mathematical Functions with Formulas, Graphs, and Mathematical Tables*. Dover, New York, ninth dover printing, tenth gpo printing edition, 1964.

[34] Bram van Leer. Towards the ultimate conservative difference scheme. v. a second-order sequel to godunov's method. *Journal of Computational Physics*, 32(1):101 – 136, 1979.

[35] A. Jameson and S Yoon. Lower-upper implicit schemes with multiple grids for the euler equations. *AIAA*, 25(7):929–935, 1987.

[36] C. Hirsch. *Numerical Computation of Internal and External Flows*. Wiley, New York, 1988.

[37] T. I. P. Shih and W. J. Chyu. *AIAA*, 29(10):1759, 1991.

[38] Se-Myong Chang and Keun-Shik Chang. On the shock vortex interaction in Schardin's problem. *Shock Waves*, 10:333–343, 2000.

[39] Tze-Yang Hsieh and Jaw-Yen Yang. Thermal conductivity modeling of circular-wire nanocomposites. *Journal of Applied Physics*, 108:044306, 2010.

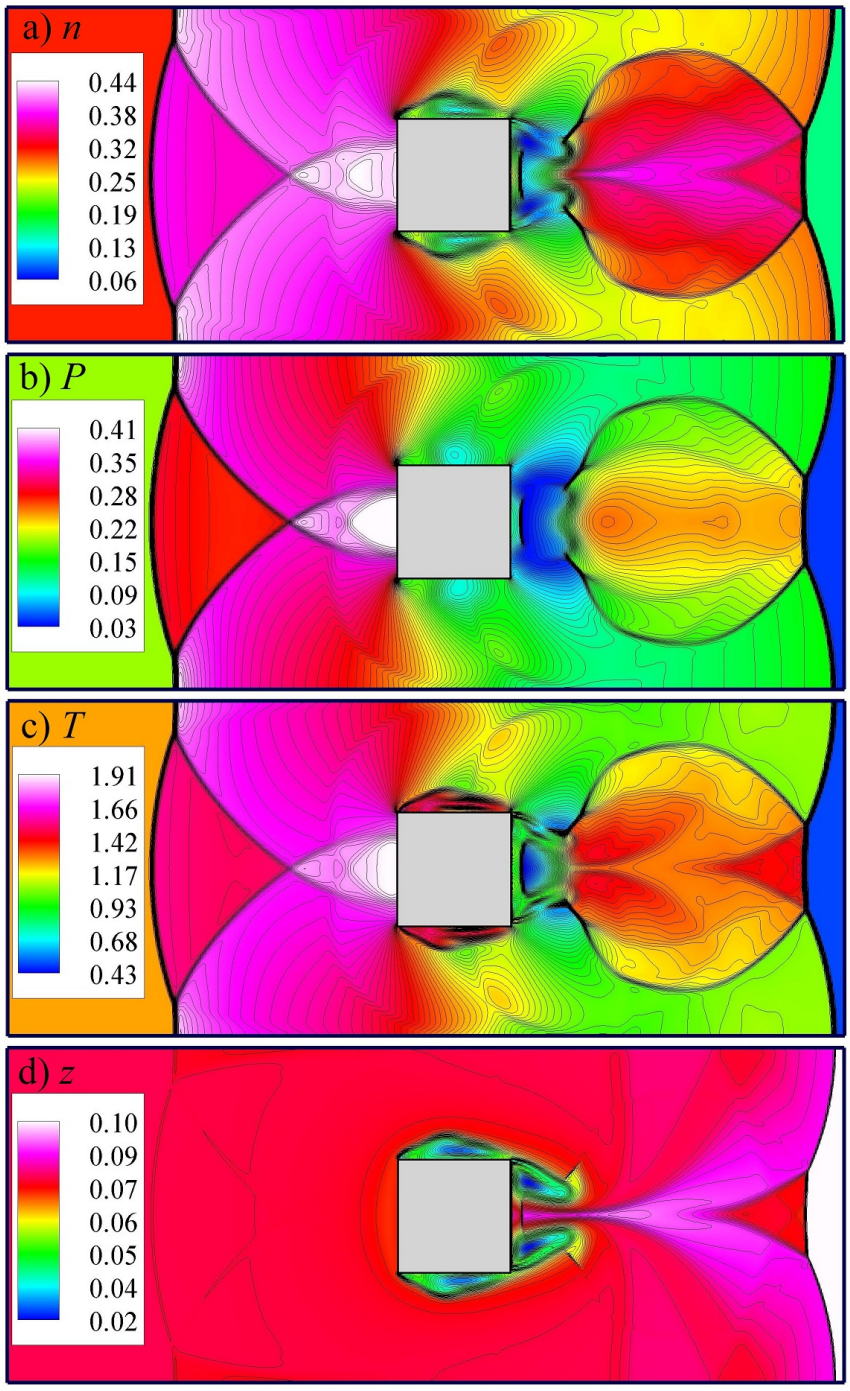

Figure 1: (a) Density, (b) Pressure, (c) Temperature and (d) Fugacity contours of diffracted gas flow in a channel

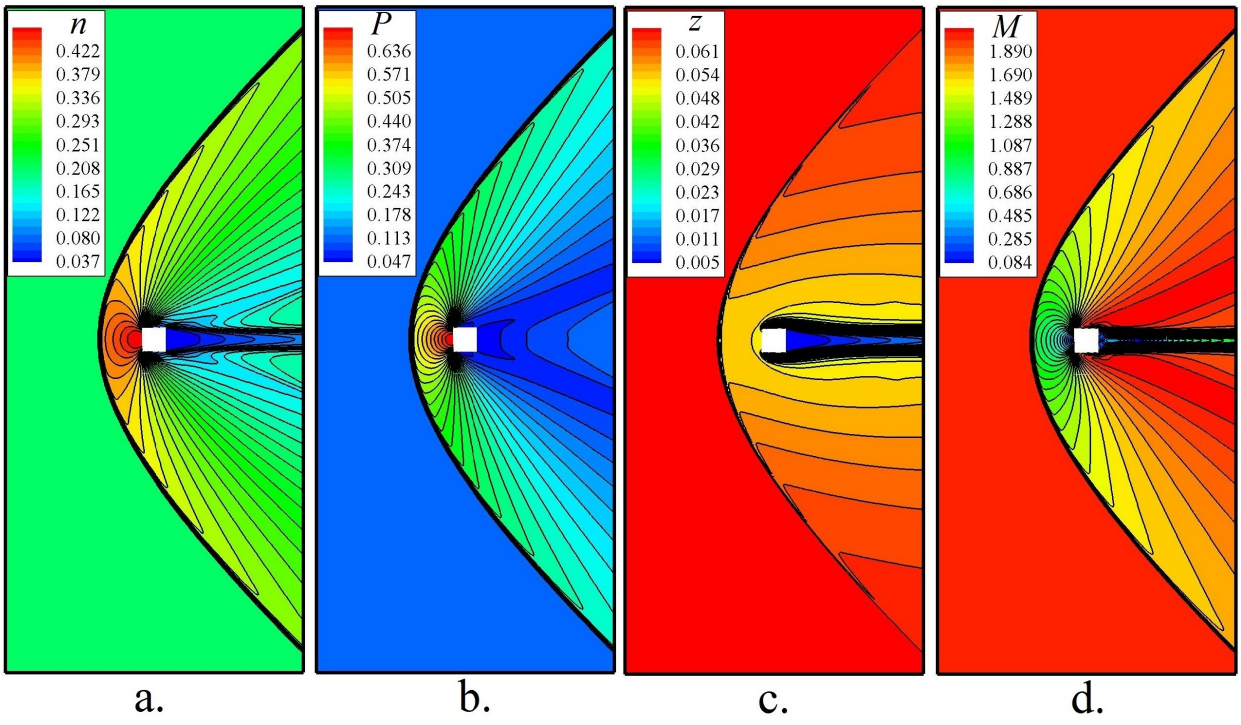

Figure 2: Supersonic flow of $M_\infty = 2.0$ depicting, a. Density, b. Pressure Contours, c. Fugacity and d. Mach Contours of Fermi-Dirac Gas with $\tau = 0.0005$, Kn $= 0.000511$ and $M_\infty = 2.0$

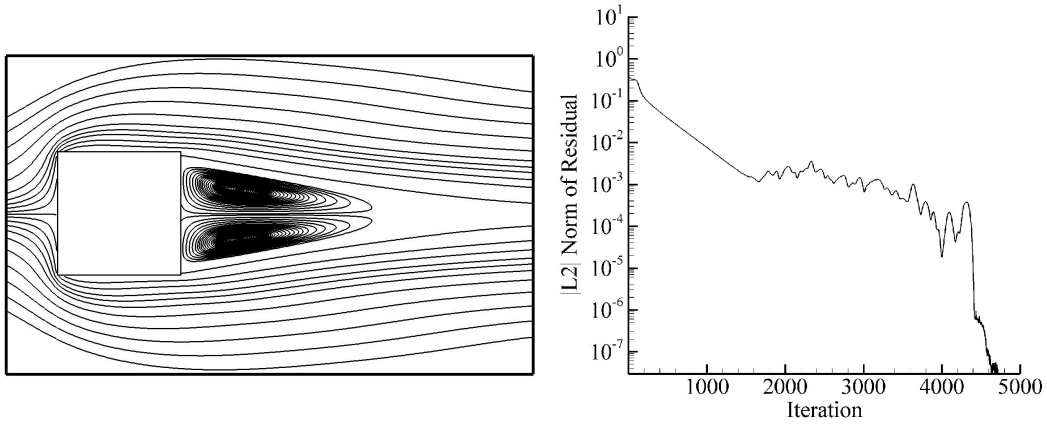

Figure 3: (left) Streamline of Fermi-Dirac Gas near Continuum Regime with $\tau = 0.0005$, Kn $= 0.000511$ and $M_\infty = 2.0$. (right) History of Residual Versus Iteration

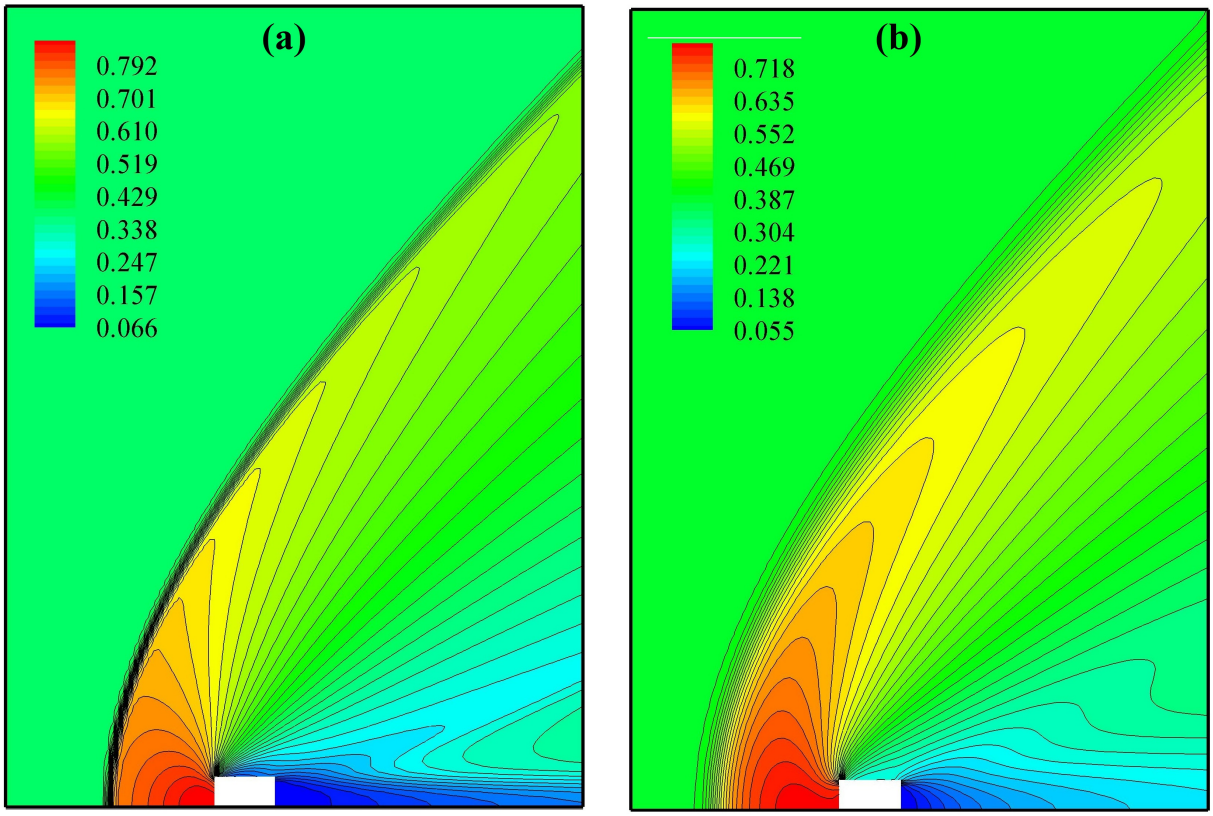

Figure 4: (a) Density contour of Bose-Einstein gas at Euler limit upon Convergence, (b) Density contour of Bose-Einstein gas with $\tau = 0.1$ (Kn $= 0.112$) at $M_\infty = 2.0$